Stressing of the ZEPHYR Vacuum Vessel by Plasma Disruptions

H. Kotzlowski, K.F. Mast, H. Preis

IPP 1/175 November 1979

MAX-PLANCK-INSTITUT FÜR PLASMAPHYSIK

8046 GARCHING BEI MÜNCHEN

MAX-PLANCK-INSTITUT FÜR PLASMAPHYSIK

GARCHING BEI MÜNCHEN

Stressing of the ZEPHYR Vacuum Vessel by Plasma Disruptions

H. Kotzlowski, K.F. Mast, H. Preis

IPP 1/175 November 1979

Die nachstehende Arbeit wurde im Rahmen des Vertrages zwischen dem Max-Planck-Institut für Plasmaphysik und der Europäischen Atomgemeinschaft über die Zusammenarbeit auf dem Gebiete der Plasmaphysik durchgeführt.

List of Symbols

A	plasma aspect ratio
B_{pol}	poloidal magnetic field
B_T	toroidal magnetic field
B_v	vertical magnetic field
d_s	thickness of single-walled shell sector
d_{s+}	thickness of double-walled shell sector
d_b	thickness of single-bellows shell sector
d_{bu}	equivalent thickness of bellows sector in toroidal direction
d_{bv}	equivalent thickness of bellows sector in poloidal direction
ℓ_p	length of poloidal vessel circumference
ℓ_b	real toroidal length of single bellows
ℓ_{bs}	toroidal length of bellows sector
N	number of bellows and shell sectors
ϱ	resistivity
τ_p	decay time of plasma current
τ_v	time constant of poloidal eddy currents
τ_0	time constant of toroidal "monopole" current
τ_1	time constant of toroidal "dipole" current

1. Introduction

To investigate the physical properties of a mainly α - particle-heated plasma, an ignition experiment, called Zephyr, is now under investigation at Garching. It is intended to reach ignition conditions by adiabatic compression of a plasma, preheated ohmically and by neutral injection.

The vacuum vessel of the Zephyr experiment has to be developed with due regard for critical boundary conditions not yet encountered together in any plasma experiment under construction (see Table I). It has to withstand severe thermal and electromagnetic loads, must not disturb the vertical field during adiabatic compression and has to meet tritium safety requirements while the distance between the toroidal field coil and the plasma edge at the vessel throat is kept as low as possible, in the range of 10 cm. Activating of the structure requires maintenance and repair under remote handling conditions.

It became clear during the design study of the vacuum vessel that an all-metal configuration without poloidal insulating gaps, separated from the toroidal field coils, would be the best solution, provided that the type-wound coil for the TF magnet is chosen. The concept of a thick vessel with insulating gaps was first investigated /1/, but it was not possible to find any insulating material capable of withstanding the large forces across the gap, caused by plasma disruptions. Based on that concept, the vacuum vessel is composed of double-walled bellows and thick shell sections of elliptical shape (Fig. 1). A sufficiently high toroidal electrical resistance is imposed by the bellows, which allow toroidal movements due to temperature variations. The shell sections, linked to the TF magnet, form the supporting structure and incorporate the ports for neutral injection, pumping and diagnostics. A thin-walled vessel without thick shell sections entails problems with the large openings for neutral injection and needs a lot of connections with the cases of the TF coils.

Eddy currents, induced in the vessel wall by transient magnetic fluxes, exert large forces on the vessel by interacting with the magnetic fields, mainly with the stationary toroidal magnetic field. Especially the electromagnetic forces, caused by a hard plasma disruption of the compressed plasma have a major influence on the vessel design.

It is therefore necessary to calculate these forces for a variety of different geometries of the chosen vessel concept, e.g. for different plasma aspect ratios A, during the design phase of the vessel for deriving scaling laws. The methods mostly used to determine eddy current distributions are either analytical calculations, which are not accurate for such a complicated structure, or extensive FE calculations.

A numerical-analytical computation method was therefore developed, yielding sufficiently accurate results for a limited outlay. Recent calculations with a FE code /2/ show good agreement with the results of the described calculation method.

This report first describes in Sec. II the features of the current eigenmodes in the vessel. The most important modes caused by hard disruption of the plasma current, are derived in Sec. III from these results. The method of calculating these modes is then represented and results for the two plasma aspect ratios A = 2.7 and A = 3.5 are compared. Simple scaling laws, describing the variation of the electromagnetic forces with the aspect ratio of the compressed plasma, are described in Sec. IV. The resulting electromagnetic forces are then used as input for the stress analysis of the vacuum vessel using a finite element program. The results are discussed in Sec. V.

II. Eddy Currents on the Vacuum Vessel

The eddy currents on the vacuum vessel are calculated, assuming that the vessel can be represented as a thin shell, e.g. no current flows in the direction normal to the vessel surface. This assumption is justified since any radius of curvature of the vessel is much larger than the wall thickness.

Any shape of vessel surface can then be described by a two-dimensional orthogonal system of coordinates (u, v) which is related to a Cartesian system of coordinates (X_1, X_2, X_3) by

$$X_i = X_i(u, v) \qquad i = 1, 2, 3 \tag{1}$$

The surface current density j can be written in the form

$$\vec{j}(u, v, t) = j_u(u, v, t)\,\vec{e}_u + j_v(u, v, t)\,\vec{e}_v \tag{2}$$

with

$$e_{u_i} = \frac{1}{f(u,v)} \cdot \frac{\partial x_i}{\partial u} \qquad e_{v_i} = \frac{1}{g(u,v)} \cdot \frac{\partial x_i}{\partial v} \tag{3}$$

$$f(u,v) = \left[\frac{\partial x_i}{\partial u} \cdot \frac{\partial x_i}{\partial u}\right]^{\frac{1}{2}} \qquad g(u,v) = \left[\frac{\partial x_i}{\partial v} \cdot \frac{\partial x_i}{\partial v}\right]^{\frac{1}{2}} \tag{4}$$

The surface current density is divergence-free

$$\operatorname{div} j = \frac{1}{f \cdot g}\left[\frac{\partial}{\partial u}(g \cdot j_u) + \frac{\partial}{\partial v}(f \cdot j_v)\right] = 0 \tag{5}$$

and can therefore be represented by a scalar current potential $V(u, v)$ /3/

$$j_u = \frac{1}{g} \cdot \frac{\partial V}{\partial v} \qquad j_v = -\frac{1}{f} \cdot \frac{\partial V}{\partial u} \tag{6}$$

Any eddy current distribution on the vessel surface can be represented by a series of orthogonal eigenmodes

$$\vec{j}(u, v, t) = \sum_{n=0}^{\infty} \vec{j}_n(u, v) \cdot e^{\lambda_n \cdot t} \cdot a_n(t) \tag{7}$$

The coefficients $a_n(t)$ are time independent, when no coupling between the vessel

and other conductors exists.

Each eigenmode $\vec{j}_n(u,v)$ can be derived from the energy balance equation on the vessel surface

$$\frac{d\,W_M}{dt} + P = 0 \tag{8}$$

The magnetic energy of the eddy currents on the vessel is described by a surface integral

$$W_M = \frac{1}{2}\oint_S \vec{j}\cdot\vec{\mathcal{A}}\,dS = \frac{\mu_0}{8\pi}\oint_{S_1}\oint_{S_2}\frac{\vec{j}_n(u_1,v_1)\cdot\vec{j}_n(u_2,v_2)}{|\vec{r}(u_1,v_1)-\vec{r}(u_2,v_2)|}\,dS_2\,dS_1 \tag{9}$$

and the ohmic loss per unit time by

$$P = \oint_S \vec{j}\cdot\overleftrightarrow{\varrho}\cdot\vec{j}\,dS = \oint_S j_u(\varrho_u\cdot j_u + \varrho_{uv}\cdot j_v) + j_v(\varrho_{uv}\cdot j_u + \varrho_v\cdot j_v)\,dS \tag{10}$$

$$\overleftrightarrow{\varrho} = \begin{pmatrix} \varrho_u(u,v) & \varrho_{uv}(u,v) \\ \varrho_{uv}(u,v) & \varrho_v(u,v) \end{pmatrix} \tag{11}$$

On the bellows sectors, the resistivity becomes a symmetrical matrix.

Inserting eqs. (2), (10) and (9) in eq. (8) yields a system of two coupled, homogeneous integral equations of the Fredholm type

$$\lambda_n\cdot\oint_{S_2}\overleftrightarrow{W_M}(1,2)\cdot\vec{j}_n(2)\,dS_2 + \overleftrightarrow{\varrho}(1)\cdot\vec{j}_n(1) = 0 \tag{12}$$

The index 1 denotes the coordinates (u_1, v_1), the index 2 (u_2, v_2):

$$\overleftrightarrow{W_M}(1,2) = \begin{Bmatrix} \vec{e}_u(1)\cdot\vec{e}_u(2) & \vec{e}_u(1)\cdot\vec{e}_v(2) \\ \vec{e}_v(1)\cdot\vec{e}_u(2) & \vec{e}_v(1)\cdot\vec{e}_v(2) \end{Bmatrix}\cdot\frac{\mu_0}{4\pi|\vec{r}(u_1,v_1)-\vec{r}(u_2,v_2)|} \tag{13}$$

By multiplying eq. (12) by $\vec{j}_m(1)$ and integrating over the vessel surface with index 1, it can be shown that the eigenvalues λ_n are real and negative. Using the same scalar products for two different eigenmodes with index m and n, it can be shown that the eigenmodes are normalized by

$$\oint_{S_1}\oint_{S_2} \vec{j}_m(1) \cdot \overleftrightarrow{W_M}(1,2) \cdot \vec{j}_n(2)\, dS_2\, dS_1 = \delta_{mn} \qquad (14)$$

The eigenmodes are therefore energetically decoupled and are given by

$$\vec{j}_n(u,v,t) = \vec{j}_n(u,v) \cdot e^{\lambda_n \cdot t} \qquad (15)$$

The symmetry properties of the vessel are valid for the eigenmodes, too. They are symmetrical to the meridian plane of the vessel and to the vertical symmetry planes of each shell and bellows sector, while the toroidal periodicity is given by $\Delta\varphi = 2\pi/N$ (N = number of bellows or shell sectors).

III. Eigenmodes and Electromagnetic Loads Induced by Hard Plasma Disruption

The most critical electromagnetic loads on the vessel, far exceeding the atmospheric pressure, are induced by hard disruption of the compressed plasma. Very little is known about the time behaviour of the plasma current during its decay interval. But it seems that inside a vacuum vessel with a copper shell most hard disruptions occur during a time interval of several milliseconds (Pulsator, FT-tokamak), while the number of disruptions with durrent decay time shorter than one millisecond increases for vessels without copper shell.

In both cases, the vessels must be able to withstand a hard disruption with a current decay time much shorter than the toroidal and poloidal vessel time constants, e.g. nearly the entire plasma current then appears in the vessel wall.

For this worst case, the most important eigenmodes were determined and the electromagnetic loads derived from these were used as the critical input parameters for the stress analysis of the vacuum vessels for different plasma aspect ratios. In any case, only double-walled

vessels were considered.

Denoting the toroidal coordinate on the vessel surface with u and the poloidal one with v , the following important eigenmodes for an idealized vessel (Fig. 2) can be distinguished after a hard plasma disruption, fulfilling the conditions

$$\tau_p << \tau_0 \quad ; \quad \tau_p << \tau_1 \quad ; \quad \tau_p << \tau_v \tag{16}$$

$$\vec{j}^{\,0}(u,v,t) = j_v(v) \cdot e^{-\frac{t}{\tau_v}} \cdot \vec{e}_v \tag{17}$$

caused by the diamagnetic plasma

$$\vec{j}^{\,(0)}(u,v,t) = j_u^{(0)}(v) \cdot e^{-\frac{t}{\tau_0}} \cdot \vec{e}_u \tag{18}$$

induced by the transient component of the poloidal magnetic field, tangential at the vessel surface. This zero-order mode has to meet the condition

$$\oint \vec{\chi} d\vec{s} = \oint \vec{\varrho} \cdot \vec{j} d\vec{s} = 0$$

at the vessel surface .

$$\vec{j}^{\,(1)}(u,v,t) = \left[j_u^{(1)}(v) \cdot \vec{e}_u + j_u^{(s)}(u,v) \cdot \vec{e}_u + j_v^{(s)}(u,v) \cdot \vec{e}_v \right] \cdot e^{-\frac{t}{\tau_1}} \tag{19}$$

induced by the transient component of the poloidal magnetic field, normal to the vessel surface.

In each shell and bellows sector, there flow so-called saddle currents $\vec{j}_s = \left(j_u^{(s)} \cdot \vec{e}_u + j_v^{(s)} \cdot \vec{e}_v \right) \cdot e^{-\frac{t}{\tau_1}}$ forming closed current loops on the upper and lower vessel halves. They are ohmically and inductively coupled mutually and with the dipole current $j_u^{(1)} \cdot \vec{e}_u$. There may exist current modes of higher order on a vessel surface, but they can be neglected for the chosen vessel concept (Fig. 1) for a hard disruption in the compressed plasma state under the conditions (16), as is shown later.

a) Eddy Currents Induced by Transient Toroidal Magnetic Fields Caused by a Diamagnetic Plasma

In the compressed plasma state the toroidal magnetic flux inside the vessel Φ_T is smaller than it would be without plasma since $\beta_p > 1$.

$$\Phi_T < \int_{F_v} \frac{C_1}{R}\, dF$$

F_v = vessel cross-section

$B_T = \frac{C_1}{R}$ = toroidal magnetic field in the vacuum.

The negative magnetic flux difference

$$\tilde{\Phi}_T = \Phi_T - \int_{F_v} \frac{C_1}{R}\, dF < 0 \qquad (20)$$

marks a diamagnetic plasma.

With the assumption $\tau_p << \tau_v$ the toroidal magnetic flux $\Delta\Phi_T \approx \tilde{\Phi}_T$ diffuses into the vessel after disruption, inducing large poloidal eddy currents nearly equal to the diamagnetic plasma current.

The axisymmetric mode which is the most important one can be derived by expanding all quantities in Fourier series of the toroidal variable .

With $u = \varphi$, $v = v(R)$ (Fig. 2) the poloidal current density on the idealized vessel can be written as

$$j_v(\varphi, R, t) = \left[a_0(t) + a_1(t) \cdot \cos(N\varphi)\right] \cdot \frac{1}{R} \qquad (21)$$

and the wall thickness in the poloidal direction $d(\varphi)$ as

$$d(\varphi) = d_0 + d_1 \cdot \cos(N\varphi) \qquad (22)$$

$$d_0 = \frac{d_{bv} \cdot \varphi_b + d_s^+ \cdot \varphi_s}{\varphi_b + \varphi_s} \qquad (23)$$

$$d_{bv} = 2 \cdot d_b \cdot \frac{\ell_b}{\ell_{bs}} \qquad (24)$$

$$d_{bu} = 2 \cdot d_b \cdot \frac{\ell_{bs}}{\ell_b} \qquad (25)$$

$$\frac{\ell_b}{\ell_{bs}} = \text{const}(R) \qquad (26)$$

Using $(rot\, \dot{\gamma}_0)_u = -\dot{\mathcal{E}}_{0u}$ for the zero-order coefficients (with index 0) of the Fourier series, the differential equation for $a_0(t)$ is given by

$$-\mu_0 \int_{F_v} \frac{1}{R}\, dF \cdot \frac{da_v}{dt} = \frac{\rho}{d_0} \oint \frac{1}{R} \cdot g(v)\, dv \cdot a_0(t) \qquad (27)$$

with the result

$$j_v(\varphi, R, t) = \frac{1}{\mu_0} \cdot \frac{\tilde{\Theta}_T}{\Theta_{T_v}} \cdot B_T(R) \cdot e^{-\frac{t}{\tilde{\tau}_v}} \qquad (28) \qquad \Theta_{T_v} = \int_{F_v} B_T(R)\, dF \qquad (29)$$

$$\tilde{\tau}_v = \frac{d_0 \mu_0}{\rho} \cdot \int_{F_v} \frac{1}{R}\, dF \cdot \left[\oint \frac{g(v)}{R}\, dv \right]^{-1} \qquad (30)$$

The poloidal current j_v interacts with the toroidal magnetic field yielding a magnetic pressure p_{M_n} normal to the vessel surface

$$p_{M_n} = \frac{1}{\mu_0} \cdot \frac{\tilde{\Theta}_T}{\Theta_{T_v}} \cdot B_T^2(R) \cdot e^{-\frac{t}{\tilde{\tau}_v}} \qquad (31)$$

The diamagnetic flux $\tilde{\Theta}_T$ can be estimated sufficiently accurate from a cylindrical plasma model ($A \to \infty$), as $\beta_p \leq \frac{A}{2}$.

Assuming a plasma current profile

$$j(r) = j_0 \left(1 - \left(\frac{r}{a}\right)^2\right)^2 \qquad a = \text{plasma radius} \qquad (32)$$

and a quadratic pressure profile

$$p(\psi) = A_1 \cdot \psi^2 \qquad (33)$$

with the poloidal magnetic flux function $\psi(r) = \int_{r=0}^{r} B_{pl}(r)\, dr$, $\tilde{\Theta}_T$ can be calculated by using the plasma equilibrium equation

$$\frac{dp}{dr} = -\frac{1}{2\mu_0} \cdot \frac{d}{dr} B_z^2(r) - \frac{1}{\mu_0} \cdot \frac{B_{pl}(r)}{r} \cdot \frac{d}{dr}\left(r \cdot B_{pl}(r)\right) \qquad (34)$$

as

$$\tilde{\Theta}_T = \frac{\mu_0^2}{8\pi} \cdot \frac{(1-\beta_p)}{B_T} \cdot I_{pl}^2 \qquad (35)$$

$$\beta_p = \frac{\langle p \rangle \cdot 2\mu_0}{B_{pa}^2} \qquad (36)$$

$$A_1 = \frac{105 \cdot \beta_p}{22\, \mu_0 \cdot a^2} \qquad (37)$$

Two different vessel geometries compatible with the plasma aspect ratios A = 3.5 and A = 2.7 (Table II) were investigated to derive the dependence of the eddy currents and the electromagnetic forces on A.

To calculate $\tilde{\Theta}_T$, the toroidal magnetic field on the plasma axis was inserted in eq. (35). The results are presented in Table III.

The maximum pressure load p_{Mn}^{max} occurs at t = 0 at the vessel throats R = R_i.

	A = 3.5	A = 2.7
β_p	1.75	1.35
I_{pl}	2.7×10^6 A	3.6×10^6 A
B_T	12.3 T	9.5 T
$\tilde{\Theta}_T$	-2.8×10^{-2} Vs	-2.9×10^{-2} Vs
$p_{Mn}^{max}(R_i)$	0.5×10^6 Pa	0.4×10^6 Pa

Table III

The first-order Fourier coefficients are small with respect to the zero-order one since $\frac{d_s^+}{d_{bv}} \leq 1.6$.

On the real vessel the eigenmodes are somewhat disturbed since the orthogonal system of coordinates (u', v') does not agree with the toroidal system of coordinates (u, v) (Fig. 3). But in any case the values of the maximum pressure loads are still valid ($\tau_p << \tau_v$), while the time constant τ_v is a little changed.

If the maximum electromagnetic loads caused by the diamagnetism are used for the stress calculations the described model forms a good basis for the vessel design.

b) Eddy Currents Induced by Transient Poloidal Magnetic Fields

The transient poloidal magnetic fields caused by hard plasma disruption induce toroidal and poloidal eddy current distributions on the vessel, as are described by eqs. (18) and (19). With the conditions $\tau_p \ll \tau_0$ and $\tau_p \ll \tau_1$ the whole toroidal eddy current nearly reaches the value of the plasma current, and the eddy current distribution is not affected by any motion of the magnetic axis of the plasma during a disruption.

To get the worst case of electromagnetic loading of the vessel the interaction of the plasma and the eddy currents with the outer conductors, such as the OH, VF and TF coils was neglected; taking it into consideration would only slightly diminish the loads ($\tau_p \ll \tau_0, \tau_1$).

As already mentioned, the toroidal coordinates (u,v) do not agree with the orthogonal coordinates (u',v') for the real vessel geometry (Fig. 3). The two eigenmodes of eqs. (18) and (19) are therefore strongly coupled, mainly ohmically by the cylindrical bellows sectors. As the current decay time τ_p is smaller than the vessel time constants the large toroidal eddy current acts like an intrinsic current source, driving the saddle currents by the voltage drop across the bellows sectors.

On both the shell and bellows sectors the toroidal eddy currents j_φ can be separated into two components:

$$j_\varphi(R,t) = j^{(0)}_{\varphi_{s,b}}(R,t) + j^{(1)}_{\varphi_{s,b}}(R,t) \tag{38}$$

with

$$j^{(1)}_{\varphi_{s,b}}(R,t) = \sum_{m=1}^{\infty} g^{s,b}_m(t) \cdot \cos\left(2\pi \cdot m \cdot \frac{\ell}{\ell_p}\right) \tag{39}$$

by using the relations

$$\oint j^{(0)}_{\varphi_{s,b}}(R,t)\,d\ell = \oint j_\varphi(R,t)\,d\ell \tag{40}$$

(the line integral being taken along the poloidal circumference, thus yielding the entire toroidal eddy current at any moment).

and $\oint \vec{j}^{(0)}_{\varphi_{s,b}} \cdot \vec{dS} = 0$ on each bellows and shell surface.

The components $\dot{\jmath}^{(1)}_{\varphi s}$ and $\dot{\jmath}^{(1)}_{\varphi b}$ are different, as is shown in Fig. 7 for A = 2.7 and $\tau_p = 10^{-5}$ s.

The modes of eqs. (18) and (19) are therefore coupled together. A simple circuit model of a vessel sector describing the ohmic coupling of the dipole components (m = 1) of $\dot{\jmath}^{(1)}_{\varphi s,b}$, is shown in Fig. 4.

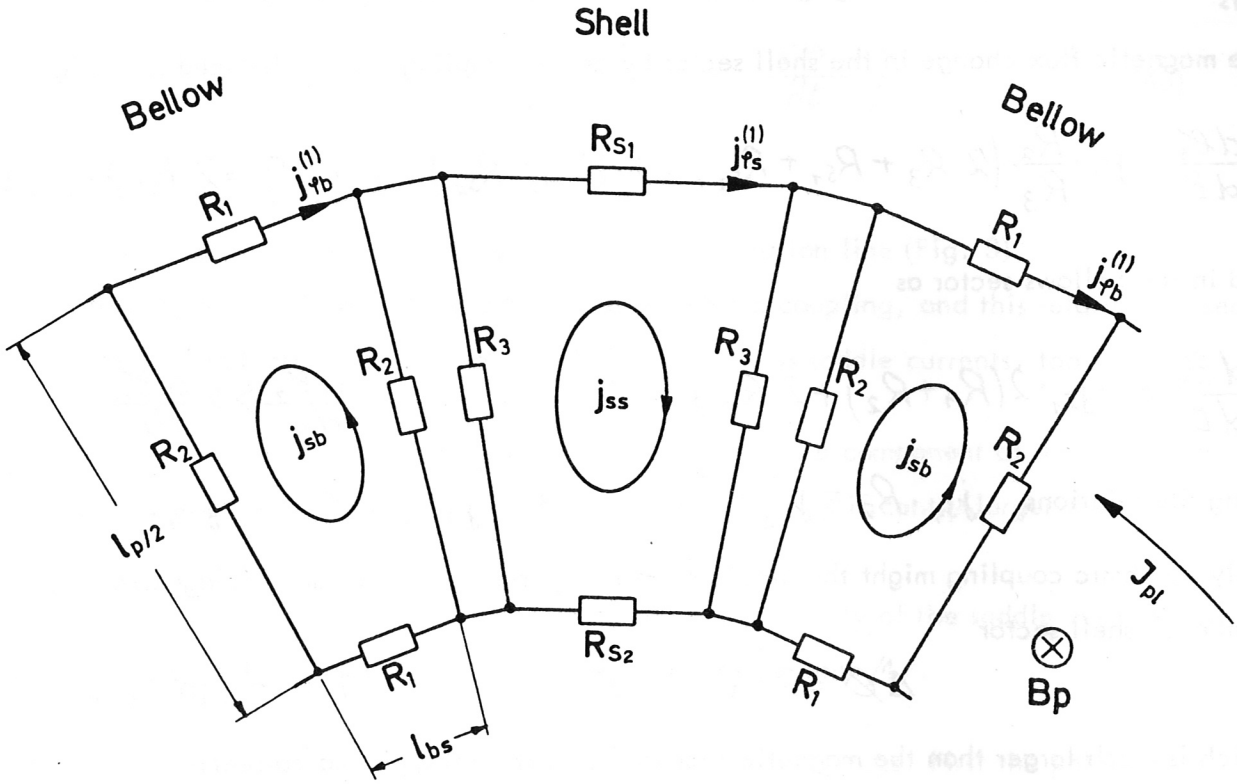

Fig. 4: Resistance circuit model of a vessel sector

$$R_1 = \frac{2 \cdot \varrho \cdot l_b}{d_b \cdot l_p}$$ = toroidal resistance of bellows sector

$$R_2 = \frac{\varrho \cdot \ell_p}{2 \cdot d_b \cdot \ell_b} = \text{poloidal resistance of bellows sector.}$$

For the vessel with A = 2.7 and the data of Table II, the following relations yield

$$\frac{R_2}{R_1} = \left(\frac{\ell_p}{2\ell_b}\right)^2 \geq 20 \; ; \quad R_{S_1} \leq 0.2\, R_1 \; ; \; R_{S_2} \leq 0.1 R_1 \; ; \; \frac{R_2}{R_3} \leq 2.5$$

It can be deduced from Fig. 7 that $j_{\varphi_b}^{(1)}$ represents the most important current component of all, therefore justifying the circuit model of Fig. 4. The quadrupole component of $j_{\varphi_s}^{(1)}$ (m = 2) only plays a negligible role for the vessel geometry of Fig. 1.

The magnetic flux change in the shell sector by ohmic coupling can be deduced from Fig. 4 as

$$-\frac{d\Phi_s}{dt} = j_{s_1} \cdot \frac{R_2}{R_3}\left(2 \cdot R_3 + R_{S_1} + R_{S_2}\right) + j_2\left(R_{S_1} + R_{S_2}\right) \approx j_{s_1} \cdot 2 \cdot R_2 = 2 \cdot R_1 \cdot j_1 \qquad (41)$$

and in the bellows sector as

$$-\frac{d\Phi_b}{dt} = -j_{s_1} \cdot 2(R_1 + R_2) + 2 \cdot R_1 \cdot j_1 \approx 0 \quad \text{since} \quad \frac{d\Phi_s}{dt} >> \frac{d\Phi_b}{dt} \qquad (42)$$

using the relations $j_{s_1} \cdot R_2 = j_{s_2} \cdot R_3$ and $j_1 \cdot R_1 \approx R_2 \cdot j_{s_1}$.

Only by ohmic coupling might the dipole current j_1 remove an amount of magnetic flux $\Delta\Phi$ from each shell sector

$$\Delta\Phi = 2 \cdot R_1 \cdot j_c \cdot \tau \qquad \tau \approx 2 \times 10^{-3}\ \text{s and}$$

which is much larger than the magnetic flux stored in it by the plasma current.

The two coupled eigenmodes of eqs. (18) and (19) can be represented on the shell and bellows sectors by the formula

$$\vec{j}_{s,b}(\varphi, R, t) = \vec{j}_{\varphi}(R, t) + \vec{j}_{s,b}^{(s)}(\varphi, R, t) \qquad (43)$$

The toroidal current component j_φ and the saddle current $j^{(s)}$ are connected by the relations

$$\text{rot}\, \mathcal{E}_{s,b} = -\frac{\partial}{\partial t} \mathcal{L}_{m_{s,b}} \qquad (44) \qquad \text{and} \qquad \vec{\mathcal{E}}_{s,b} = \overleftrightarrow{\varrho}_{s,b} \cdot \vec{j}_{s,b} \qquad (45)$$

on the shell or bellows surfaces. $\overleftrightarrow{\varrho}_s$ is a scalar quantity while $\overleftrightarrow{\varrho}_b$ is represented by a symmetrical matrix which is transferred to a diagonal matrix, if a cylindrical system of coordinates is chosen on the bellows surface:

$$\overleftrightarrow{\varrho}_s = \frac{\varrho}{d_s^+}\begin{pmatrix} 1 & 0 \\ 0 & 1 \end{pmatrix} \qquad \overleftrightarrow{\varrho}_b = \varrho \cdot \begin{pmatrix} \frac{1}{d_{bu}} & 0 \\ 0 & \frac{1}{d_{bv}} \end{pmatrix} \tag{46}$$

The currents on the bellows and shell surfaces are coupled by the boundary conditions along the separation lines of the different vessel sectors

$$\left(\mathcal{E}_s - \mathcal{E}_b\right)\cdot\vec{t} = 0 \tag{47}$$

$$\left(\frac{\partial \mathcal{B}_s}{\partial t} - \frac{\partial \mathcal{B}_b}{\partial t}\right)\cdot\vec{n} = 0 \tag{48}$$

$\vec{t}$ = tangential vector along the separation line

$\vec{n}$ = normal vector on the vessel surface along the separation line (Fig. 3).

The continuity of $\dot{B}_n$ is valid owing to the strong ohmic coupling, and this relation is used to consider the inductive coupling of the shell and bellows saddle currents, too.

The saddle currents are much smaller than the toroidal dipole component of the eddy currents, and the magnetic energy stored by the toroidal currents is significantly larger than that stored by the saddle currents.

The toroidal currents can therefore be calculated independently of the saddle currents, as has already been shown analytically for a cylindrical geometry /4/.

The calculation of the eddy currents can be divided into two steps. First the poloidal distribution of the toroidal currents j_φ is computed numerically by a method, described in /1/ and /5/. The current distribution j_φ at any moment is used as input to eqs. (44), (45), (46), (47) and (48) to derive the saddle currents on the shell and bellows sectors.

To calculate j_φ , an axisymmetric vessel was modelled with a cross-section and a poloidal distribution of the toroidal resistance equal to those of the real vessel. The wall is divided into 40 axisymmetric toroidal conductors, which are inductively coupled mutually and with the plasma. Assuming a homogeneous distribution of the plasma current and no movement of

the plasma during disruption, the current decay was simulated by suddenly increasing the plasma resistance to a value high enough to get the desired current decay time τ_p .

As an example, Fig. 5 shows poloidal distributions of j_φ on the upper vessel half for A = 3.5, when the compressed plasma disrupts. Increasing the current decay time from $\tau_p = 10^{-5}$ s to $\tau_p = 10^{-4}$ s only slightly diminishes the currents. To compare vacuum vessels for plasmas with different aspect ratios, j_φ was always computed at the moment when the maximum of the total toroidal eddy current appears in the vessel wall for a current decay time $\tau_p = 10^{-5}$ s of the compressed plasma.

In Fig. 6 the poloidal distributions of j_φ are compared for A = 3.5 with $I_{pl} = 2.7 \times 10^6$ A and A = 2.7 with $I_{pl} = 3.7 \times 10^6$ A. j_φ only increases by a small amount with decreasing A since the poloidal circumference of the vessel increases with decreasing A, too.

The saddle currents on the shell and bellows elements were derived for the two plasma aspect ratios A = 3.5 and A = 2.7 from the poloidal distributions of j_φ shown in Fig. 6. Using a cylindrical system of coordinates on the bellows surfaces and a toroidal system of coordinates on the shell surfaces (Fig. 3), the ϑ - components of the saddle currents were written as

$$j_s^{(\vartheta)} = j_{s0}^{(\vartheta)}(\ell) \cdot \frac{r}{r_0} \qquad r_0 = \frac{\varphi_s}{2} \tag{49}$$

$$j_0^{(\vartheta)} = j_{b0}^{(\vartheta)}(\ell) \cdot \left(1 - \frac{2z}{\ell_{bs}}\right) \tag{50}$$

The ϑ - components of the saddle currents are antisymmetric to the vertical symmetry plane of each shell and bellows sector and a linear dependence in the φ or z direction seems to be a good approximation for the vessel with N = 16.

Inserting eqs. (49) and (50) in eqs. (44), (45), (46), (47) and (48), the ϑ - components of the saddle currents can be derived

$$j_s^{(\nu)} = \frac{\frac{d_s^+}{d_{bu}} \cdot R(\ell) \cdot \frac{d}{d\ell} j_\varphi - \frac{d}{d\ell}(R \cdot j_\varphi)}{\left(\frac{2 \cdot \gamma_0}{\ell_{bs}} \cdot R(\ell) + 1 \right)} \cdot r \qquad (51)$$

$$j_b^{(\nu)} = \frac{d_{bv}}{d_s^+} \cdot \left[\frac{\frac{d_s^+}{d_{bu}} \cdot R(\ell) \cdot \frac{d}{d\ell} j_\varphi - \frac{d}{d\ell}(R \cdot j_\varphi)}{\left(\frac{2 \cdot \gamma_0}{\ell_{bs}} \cdot R(\ell) + 1 \right)} \right] \cdot \left(1 - \frac{2 z_0}{\ell_{bs}} \right) \qquad (52)$$

$$j_{bo}^{(\nu)}(\ell) = \frac{d_{bv}}{d_s^+} \cdot j_{so}^{(\nu)}(\ell) \qquad I_\nu = \int_{r=0}^{r_0} j_s^{(\nu)} \cdot \frac{r}{r_0} \cdot R(\ell)\, dr \qquad (53)$$

The φ and z - components of the saddle currents do not appear in eqs. (51) and (52) since the j_φ component is much larger. The term proportional to $\frac{d}{d\ell} j_\varphi$ dominates and represents the influence of the dipole current $j_{\varphi_b}^{(1)}$ (m = 1) on the bellows surface. Figure 8 shows I_ν for A = 3.5 and A = 2.7.

c) Electromagnetic Loads on the Vessel

The eddy currents on the vessel interact mutually and with the toroidal and vertical magnetic fields. A distinction can be made between loads that are axisymmetric and those being anti-symmetric to the vertical symmetry planes of each shell and bellows sector. The axisymmetric forces can be divided into three components caused by

- mutual interaction of the toroidal eddy currents j_φ
- interaction of the vertical magnetic field with j_φ
- interaction of the toroidal magnetic field with the diamagnetic eddy currents.

These are shown in Fig. 9 for A = 2.7 being divided into two poloidal components tangential and normal to the vessel surface. In Fig. 10 the total axisymmetric loads for two different aspect ratios A = 3.5 and A = 2.7 are compared. The loads p_n, normal to the vessel surface, increase slightly with decreasing A, while the tangential components p_t decrease with A.

The forces antisymmetric to the vertical symmetry planes of the vessel are caused by the interaction of the toroidal magnetic field with the poloidal components of the saddle currents. Figure 11 shows the poloidal distributions of these tilting forces for A = 3.5 and A = 2.7.

As an important result the tilting forces decrease with decreasing plasma aspect ratio A. The poloidal component of the saddle current in the shell sector j_s is nearly proportional to the ratio of the shell thickness d_s^+ and the equivalent thickness in the toroidal direction of the bellows sections d_{bu} since

$$\frac{d_s^+}{d_{bu}} \cdot R(\ell) \cdot \frac{d}{d\ell} j_\varphi >> \frac{d}{d\ell}(R\, j_\ell)$$

The saddle currents and tilting forces on the shell sectors will increase by a factor of nearly two if a vessel with single-walled bellows sections is used instead ot one with double-walled bellows, while the saddle currents and tilting forces on the bellows will remain almost unchanged. But the mechanical stresses in the single-walled bellows will be doubled.

IV. Conclusions

It would be desirable to derive analytical scaling laws for the electromagnetic loads on the vessel and the mechanical stresses caused by them as a function of the aspect ratio A of the compressed plasma.

It is therefore necessary to know the variation of the plasma parameters with A, which can be deduced from the following physical constraints:

1. Condition for alpha particle confinement

$$I_{p\ell} \cdot A = const = C_2 \qquad (54)$$

2. Condition for ignition

$$a \cdot B_{To}^2 \cdot \beta = const = C_3 \qquad (55)$$

3. Stability

$$\frac{\beta_p}{A} = const = C_1 \quad (56) \text{ and} \qquad q_a = const \qquad (57)$$

The dependence of the plasma parameters on A can be written as +)

$$B_{T_0} = \frac{2\pi}{\mu_0} \cdot q_a \cdot \frac{C_3}{C_1 \cdot C_2} \cdot A \tag{58}$$

B_{T_0} = toroidal magnetic field on the plasma axis,

$$I_{pe} = C_2 \cdot \frac{1}{A} \tag{59}$$

I_{pe} = plasma current

$$a = \frac{\mu_0^2}{4\pi^2} \cdot \frac{C_1 \cdot C_2^2}{C_3} \cdot \frac{1}{A} \tag{60}$$

a = plasma minor radius

$$B_v = \frac{\pi \cdot C_3}{\mu_0 \cdot C_2} \tag{61}$$

B_v = vertical magnetic field,

and the dependence of the poloidal circumference of the vacuum vessel on A can be approximated by ++)

$$\ell_p = \ell_{p0} - \ell_{p1} \cdot A \tag{62}$$

Assuming a hard disruption of the plasma current, the maximum toroidal eddy current reaches the value of the plasma current, and the most critical electromagnetic loads will occur.

For a hard disruption the scaling laws for these loads can easily be derived:

Axisymmetric loads caused by:

mutual interaction of toroidal eddy currents

$$\vec{P_0}(A) = \frac{a_0}{A^2 \cdot [\ell_{p0} - \ell_{p1} \cdot A]^2} \tag{63}$$

+) Approximation for large aspect ratios

++) For $A > 2$

where $\vec{p}$ = force per unit area;

interaction between toroidal eddy currents and the vertical field

$$\vec{p}_1(A) = \frac{a_1}{A\,(\ell_{p_0} - \ell_{p_1} \cdot A)} \qquad (64)$$

diamagnetism

$$\vec{p}_2(A) = a_2 \cdot \frac{(1 - C_1 \cdot A)}{A} \qquad (65) \qquad \vartheta_{T_V} \approx \text{const}(A) \qquad C_1 = \frac{\beta_P}{A}$$

Loads, antisymmetric to the vertical symmetry planes (tilting forces):

$$\vec{p}(A) = a_3 \cdot (\ell_{p_0} - \ell_{p_1} \cdot A)^{-2} \qquad (66)$$

Applying the scaling laws for the electromagnetic loads (eqs. (63) to (66)) to the case A = 2.7 the single forces agree within 20% with the calculated ones, while the sum of the axisymmetric loads differs by about 50% from the exact one. This result becomes clear from Fig. (9) which shows the whole axisymmetric load to be mainly composed of two contrary forces.

Since the dependence of the vessel geometry on A can only be considered very roughly, these scaling laws cannot be very accurate.

It will therefore not be possible by using the scaling laws to determine the mechanical stresses in the vessel as a function of A. For every plasma aspect ratio, the electromagnetic loads and the mechanical stresses must be calculated by considering the vessel geometry in detail.

V. Stress Analysis

The electromagnetic forces due to plasma disruption produce the greatest mechanical stress on the Zephyr vacuum vessel, thus governing its reliability and lifetime. As their intensity, distribution and time development strongly depend on the vessel concept and material, development of the vacuum vessel can only be accomplished in steps.

The stress analysis performed described here was preceded by two steps of this iteration

process which yielded the following results:

- Designing the vacuum vessel as a self-supporting, 1 cm thick toroidal shell with two insulating gaps is ruled out owing to the extremely high shear and compression stresses on the electrical insulation (up to 800 MPa) / 1 /. The only possibility of reducing these stresses would be to increase the distance between the TF coils and plasma from 9 to 20 cm, thus altering the parameters of the experiment. A vessel without electrically insulating gaps would have to be about 1.5 mm thick to attain the minimum toroidal resistance of 1 mΩ required.
  This is not compatible with the functional requirements imposed on the vacuum vessel such as NI ports, heat shield, tritium permeation, installation, etc..

- A compromise is afforded by the structure composed of bellows and shell sections. Here the toroidal electrical resistance is essentially governed by the bellows, and the mechanical rigidity of the vessel by the shell section. As the strength analysis shows, the single-walled shell sections (H profile) are not sufficiently rigid and their strong deformation causes unacceptably high bending stresses (up to 740 MPa).

The shell sections were therefore made double-walled (Fig. 12) and linked at several parts to the TF magnet (Fig.13) and their rigidity was adapted as much as possible to the stress (Fig. 1a). The electromagnetic forces determined in Sec. IV (Fig. 14) were distributed half and half on the two vessel walls. If the atmospheric pressure is taken into account, the load on the outer wall is slightly higher.

The calculation model for the stress analysis was a FE mesh comprising 615 shell elements and 651 nodes, each with 5 degrees of freedom (Figs. 15 and 16). The analysis was performed statically, linearly and without including other electromagnetic, thermal and gravitational loads. In keeping with the different boundary conditions for symmetry and antisymmetry the calculations were done separately and then the stress tensors were added and plotted as reference stress (von Mises):

$$\sigma_{VM} = \left[\frac{1}{2}(\sigma_1 - \sigma_2)^2 + (\sigma_2 - \sigma_3)^2 + (\sigma_3 - \sigma_1)^2 + 3\tau_1^2 + 3\tau_2^2 + 3\tau_3^2\right]^{\frac{1}{2}} \quad (67)$$

and for the two-dimensional stress state:

$$\sigma_{VM} = \left[\frac{1}{2}(\sigma_1 - \sigma_2)^2 + \sigma_1^2 + \sigma_2^2 + 3\tau_1^2\right]^{\frac{1}{2}} \qquad (68)$$

From the stress distributions over the poloidal circumference (Fig. 17) and toroidal arc (Fig. 18) it can be seen that the shell sections have dimensions that provide sufficient rigidity and are very evenly loaded. The references taken were the max.permissible stresses according to ASME, S_m (for membrane) and 1.5 S_m (for membrane + bending), and the yield stress $\sigma_{0.2}$ of the design material Inconel 625. The bellows, however, are too highly stressed in their slightly curved region, which is where the maximum load is exerted. Conventions used for stress calculations are shown in Fig. 19.

As Fig. 18 shows, the two loads produce roughly equal stresses although the tilt forces are about four times as high in intensity as the symmetric forces. However, they act very locally and essentially produce shear stresses (which are uncritical), but not bending stresses. Figure 16 illustrates the type of deformation and gives its maximum values separately for the two types of load.

The foregoing results yield the following new aspects affecting the vessel concept:

- reduction of tilt forces by increasing the number of bellows and/or decreasing bellows width
- increase of bellows thickness from 2 to 2.5 mm (smaller toroidal electrical resistance)
- additional support in centre of bellows (only possible with inner or single-walled bellows)
- strong curvature of bellows in flat region (adaptation of bellows to the outer contour of the shell section, difficult remote handling of the octant joint)
- welding seams (joining the octants) have to be shifted from the centre of the bellows to the edge (genuinely modular construction not possible, but in halves that can readily be separated)
- all joints in the bellows section have to be full penetration welds (avoidance of stress concentration).

Which of these features are applied to reduce the stresses in the bellows in the fourth stage of development of the vacuum vessel for ZEPHYR will ultimately depend on their compatibility with the functional requirements.

References

/1/ "Compact Ignition Experiment" Internal Status Report prepared by IPP Garching and CNEN Frascati, September 29, 1978

/2/ U.R. Christensen "Time Varying Eddy Currents on a Conducting Surface in 3-D Using a Network Mesh Method", PPPL-1516, April 1979

/3/ A. Kameari, Y. Suzuki "Eddy Current Analysis by the Finite Element Circuit Method", Proc. of the 7th Symp. on Eng. Problems of Fusion Research, Knoxville

/4/ B. Streibl "Eddy Currents and Magnetic Forces Originating in the JET Vacuum Vessel Due to Disruptive Instability", JET-Internal Report (1978)

/5/ H. Preis "Calculation of Voltages and Currents Induced in the Vacuum Vessel of ASDEX by Plasma Disruptions", Proc. 10th SOFT Padova, Sept. 1978

Experiment	J_{pl} [10^6A]	B_T [T]	Δ [cm]	R_T [$10^{-3}\Omega$]	double-walled	thermal shield	therm. insulation	heating/cooling system	neutralinjection	non circular cross section
FT	0.5	10	10^{TC}	∞^{J}	X[C]					
TFR 600	0.6	6	6^{T}	10		X			X	
PLT	1.6	4.9	7.5^{P}	∞^{T}					X	
ALCATOR C	1.3	14	5^{T}	4.5						
ASDEX	0.5	3	17^{P}	∞^{J}			X	X	X	X
TFTR	2.5	5.2	17.5^{T}	3.0		X	X	X	X	
JET	3.8	2.7	21^{T}	0.5	X	X	X	X	X	X
JT 60	2.7	4.5	23^{P}	1.3			X	X	X	X
ZEPHYR after compression	3.7	9.1*	9^{T}	0.7	X	X	X	X	X	X

T: TF-coil, P: PF-coil; c: copper shell; J: insulating breaks
B_T: toroidal magnetic field*on axis of compressed plasma
J_{pl}: plasma current; R_T: toroidal resistance of the vacuum vessel
Δ : distance plasma-coil

Table II : Comparison of vacuum vessels

plasma	Before compression		after compression	
	A:3.5	A:2.7	A:3.5	A:2.7
minor radius	43.7 cm	57.2 cm	36 cm	46.7 cm
major radius	185.2 cm	189 cm	126 cm	126 cm

Table III

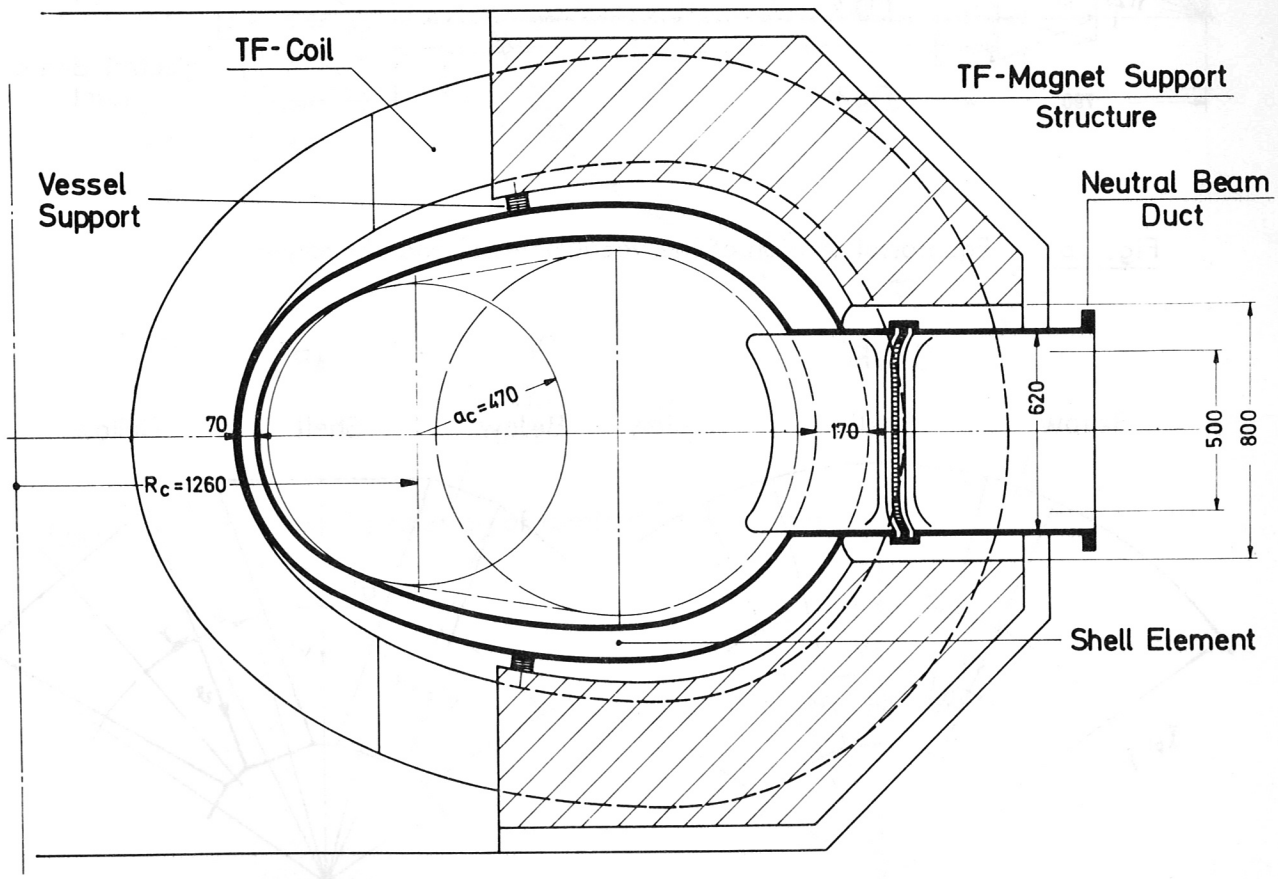

Fig. 1a: Vertical section of the vacuum vessel and TF-magnet

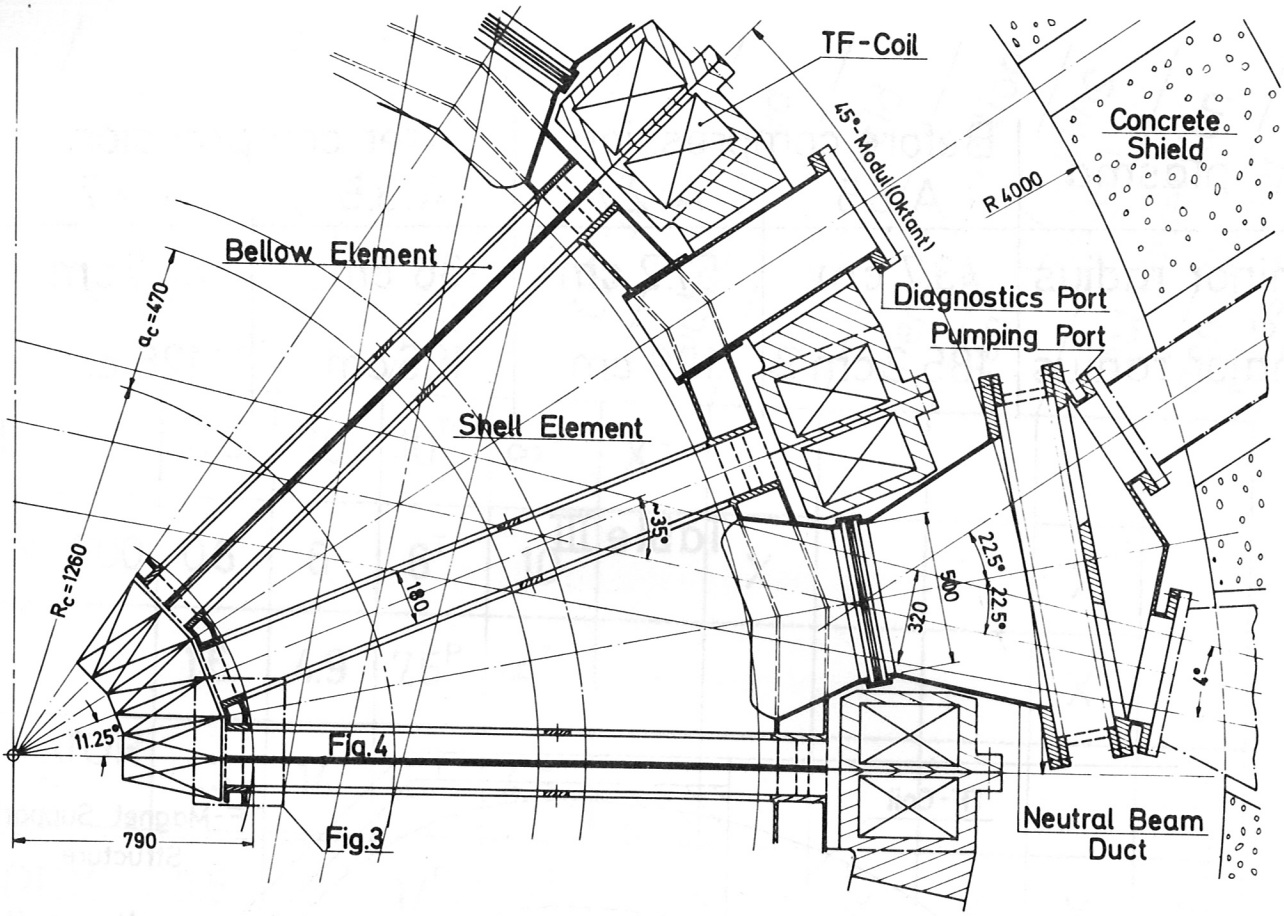

Fig. 1b: Equatorial section of the vacuum vessel and TF-magnet

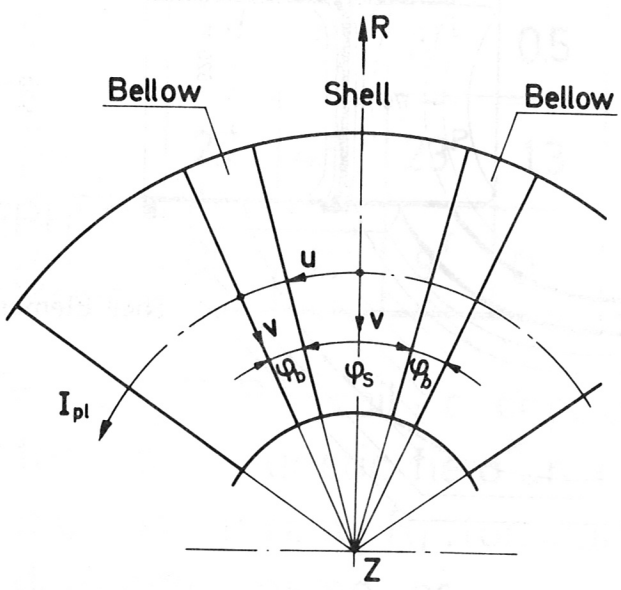

Fig. 2: Idealized vessel

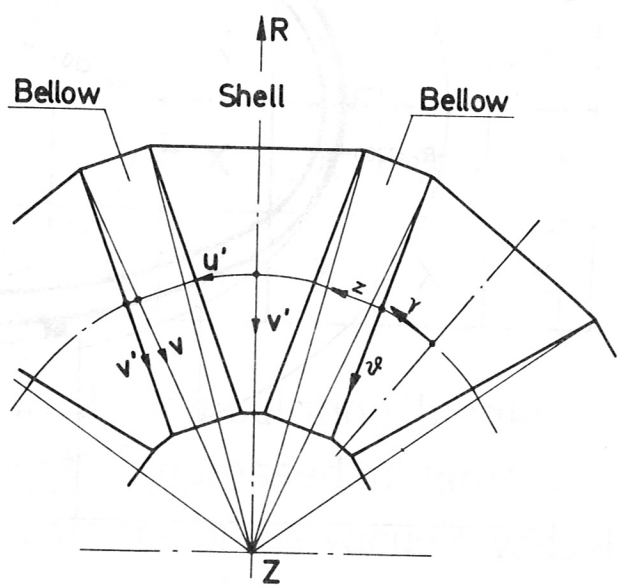

Fig. 3: Real vessel

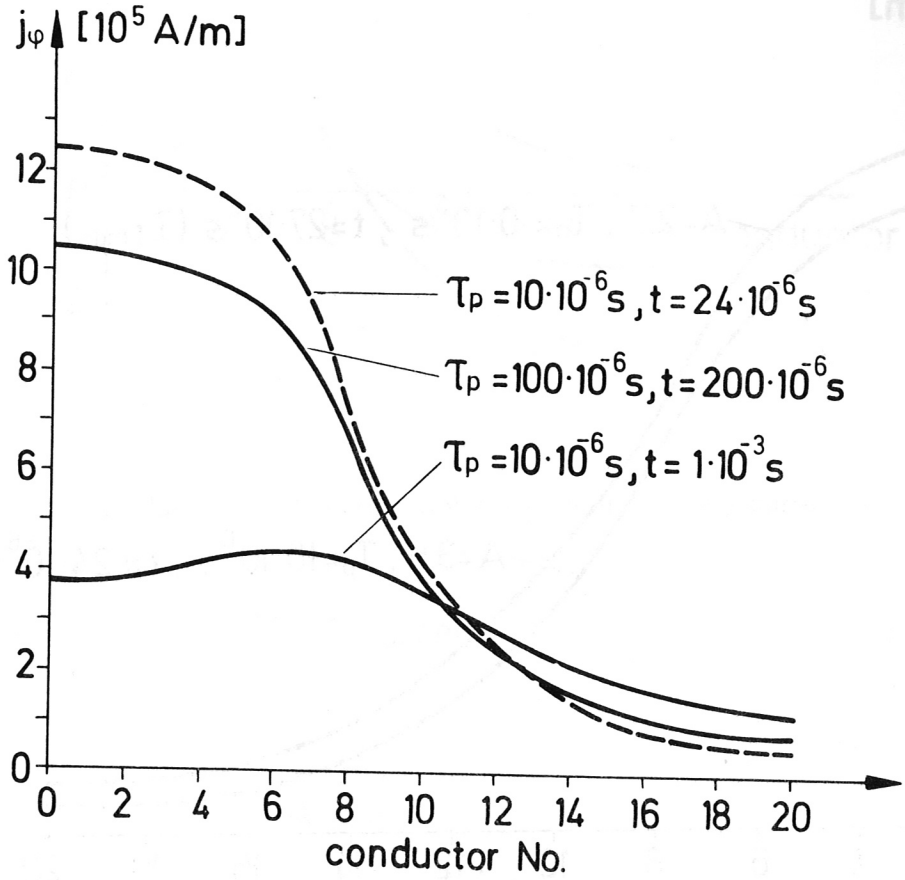

Fig. 5: Poloidal distribution of toroidal eddy currents

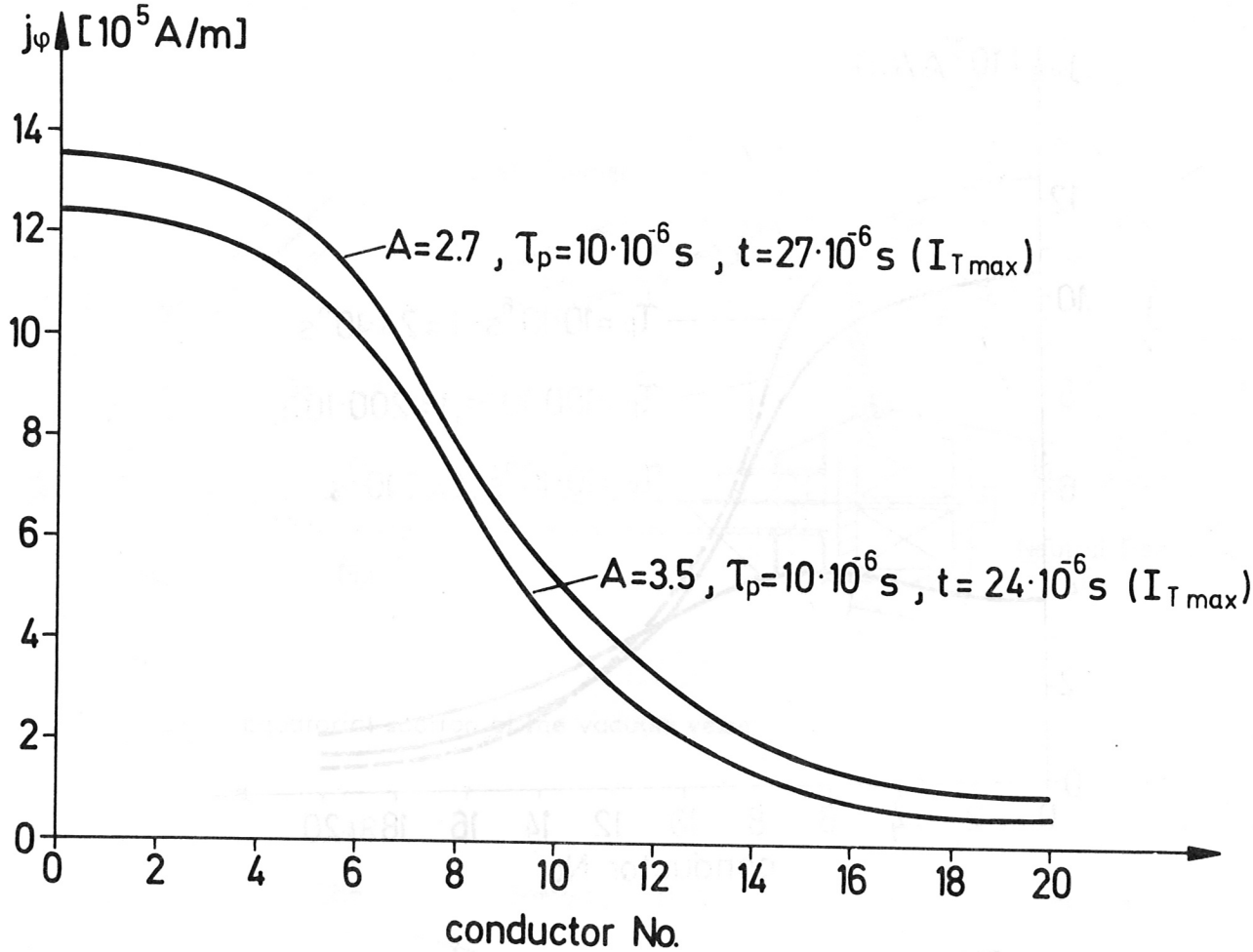

Fig. 6: Poloidal distribution of toroidal eddy currents

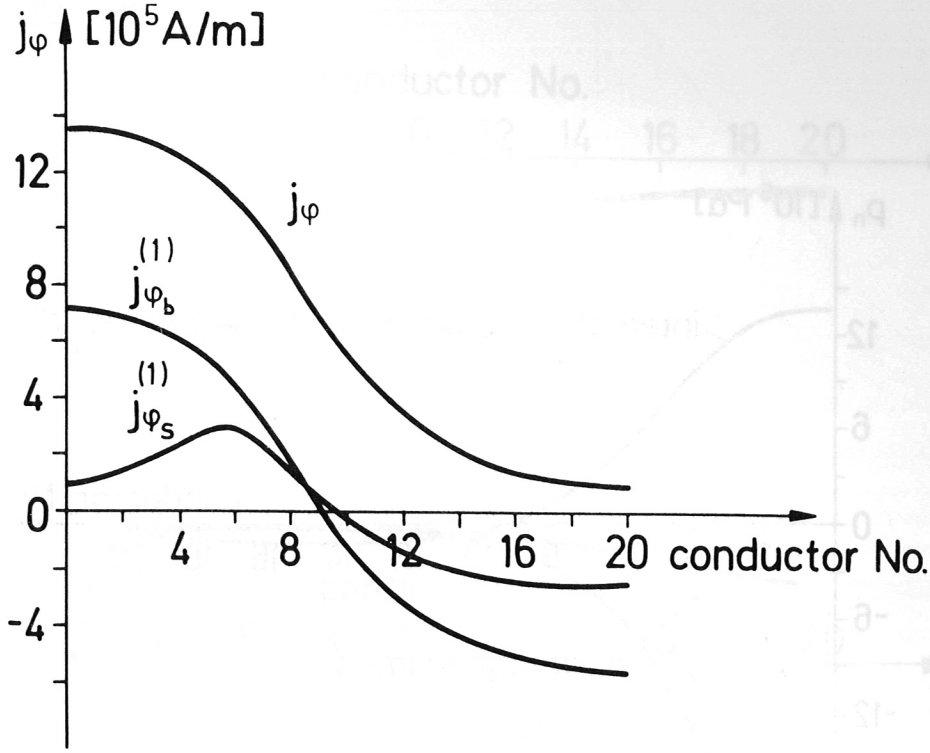

Fig. 7: Poloidal distribution of dipol components of eddy currents

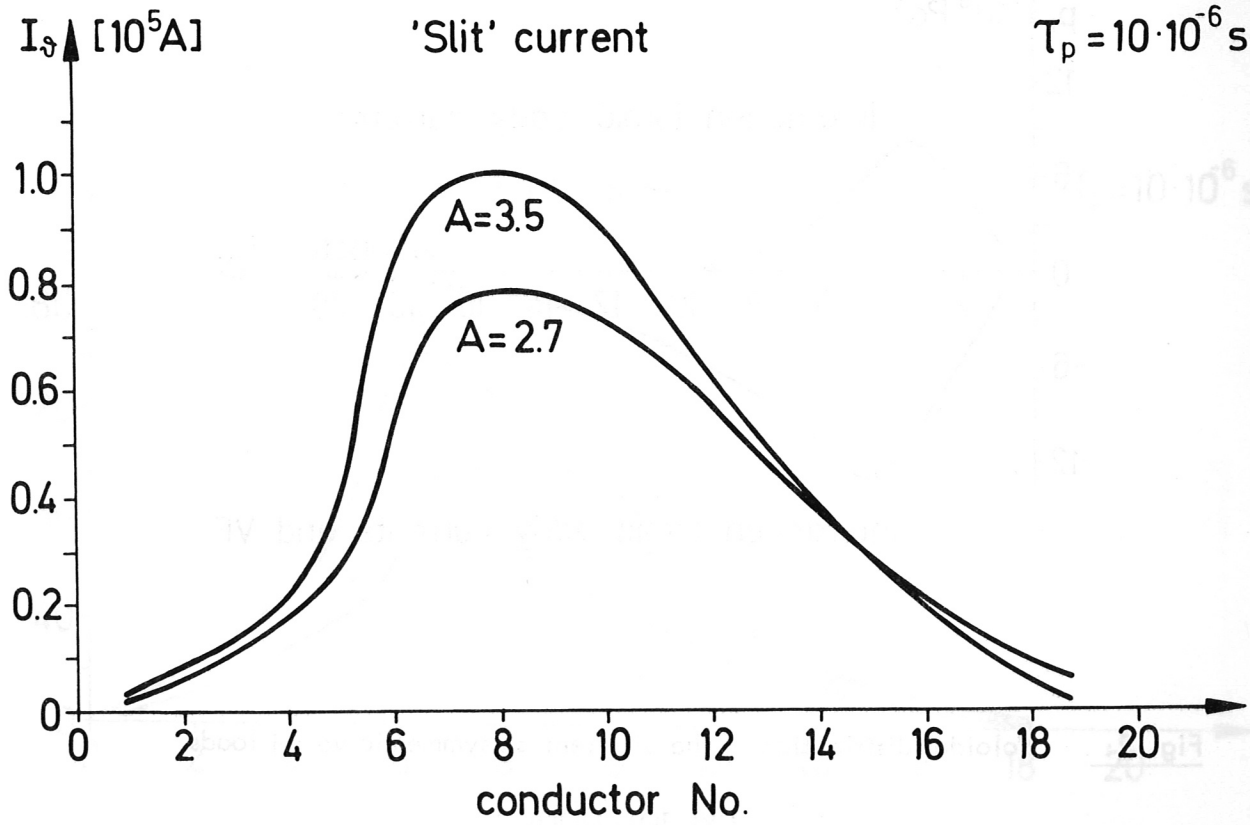

Fig. 8: Poloidal distribution of "slit" currents

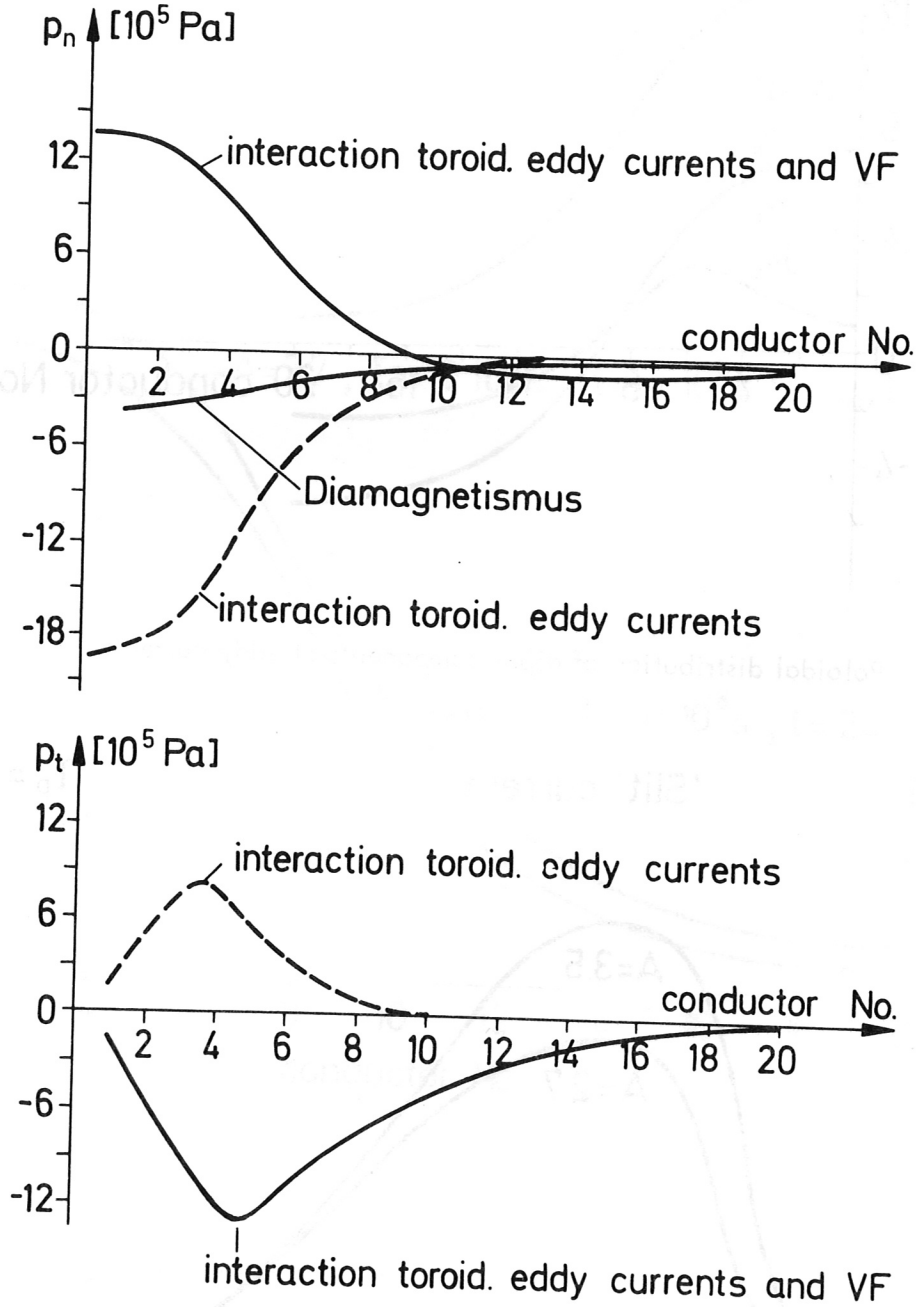

Fig. 9: Poloidal distribution of the different axisymmetric vessel loads

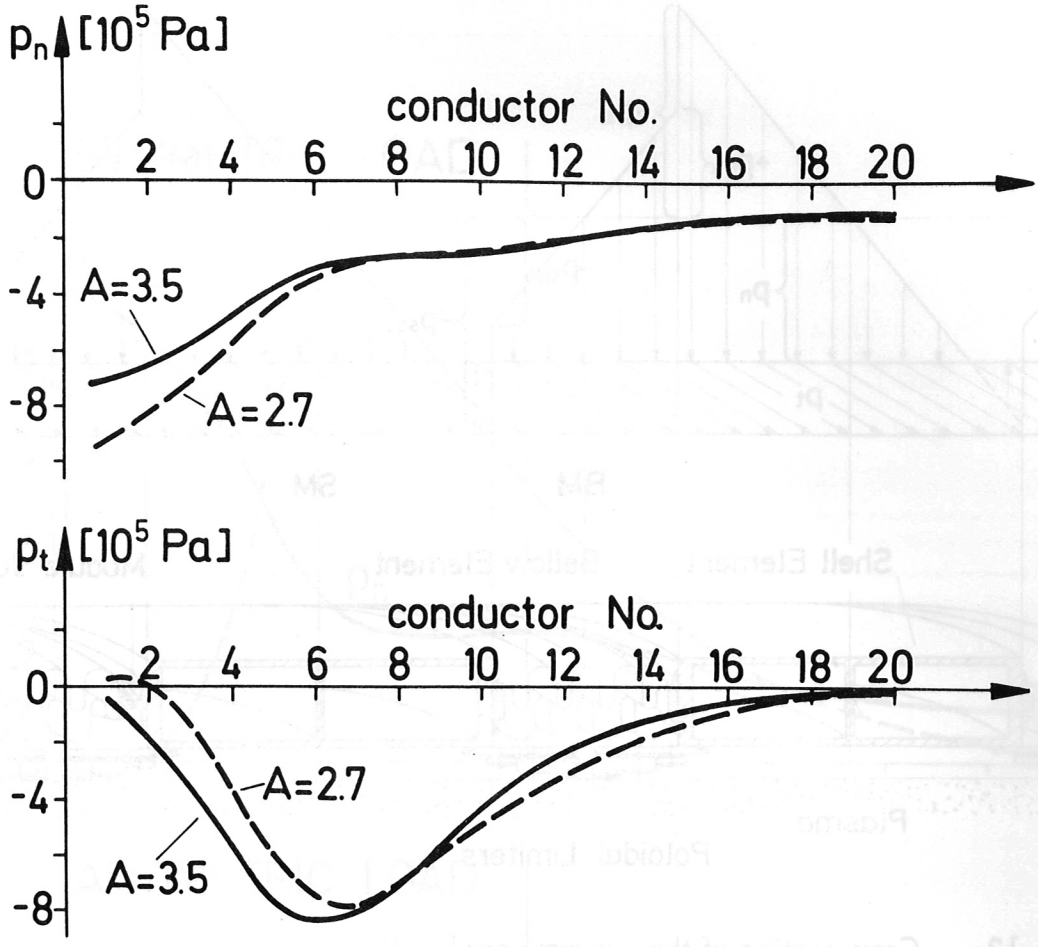

Fig. 10: Poloidal distribution of total axisymmetric vessel loads

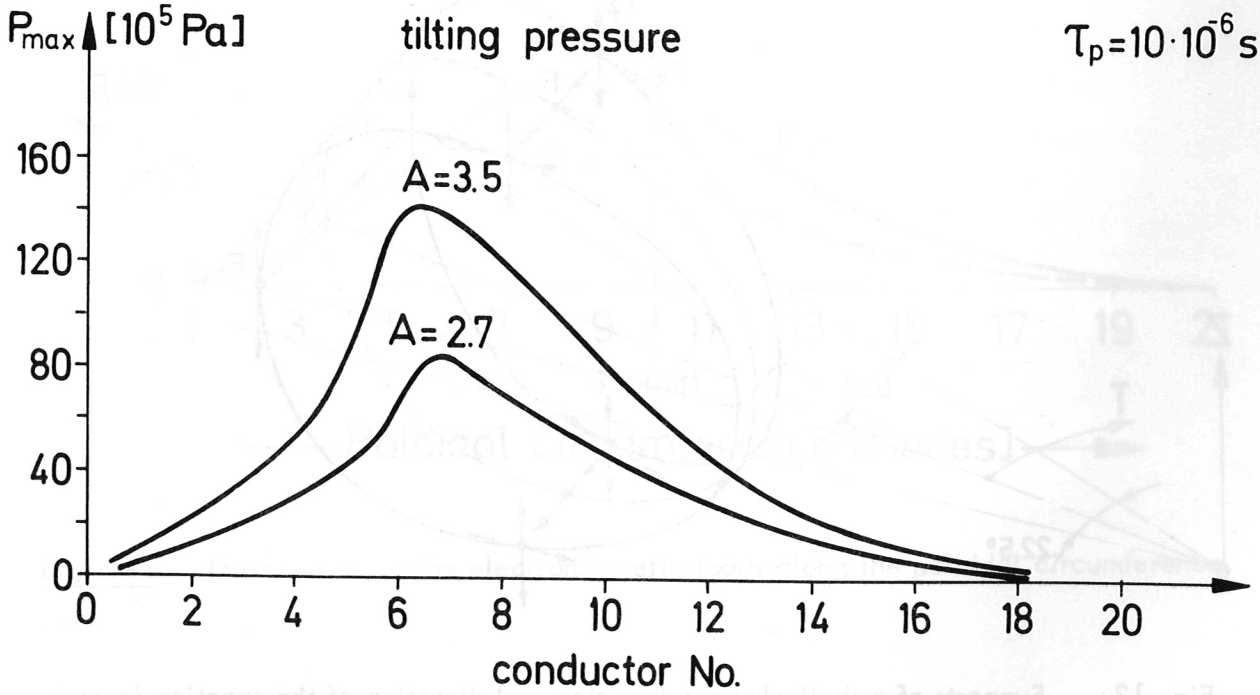

Fig. 11: Distributions of antisymmetric loads along the separation line between bellows- and shell segment

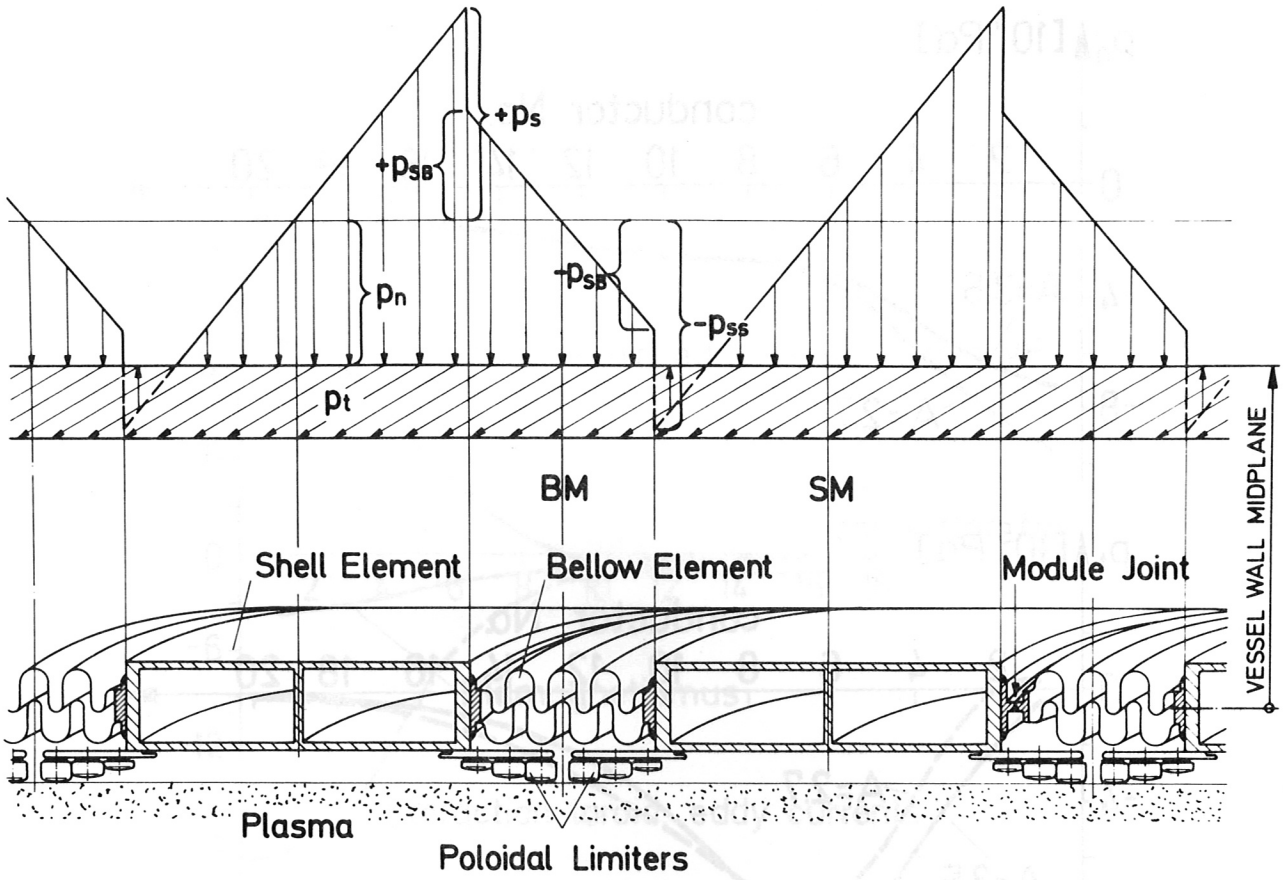

Fig. 12: Cross-section of the vacuum vessel wall.
Toroidal distribution of symmetric and antisymmetric electromagnetic loads

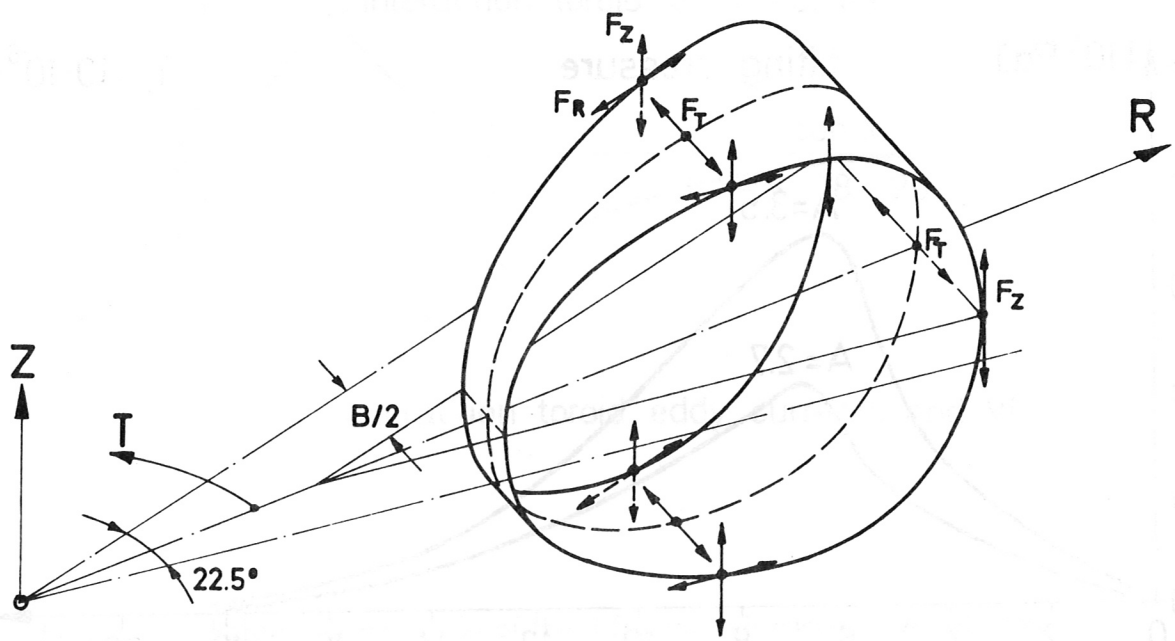

Fig. 13: Supports of a shell element (position and direction of the reaction forces)

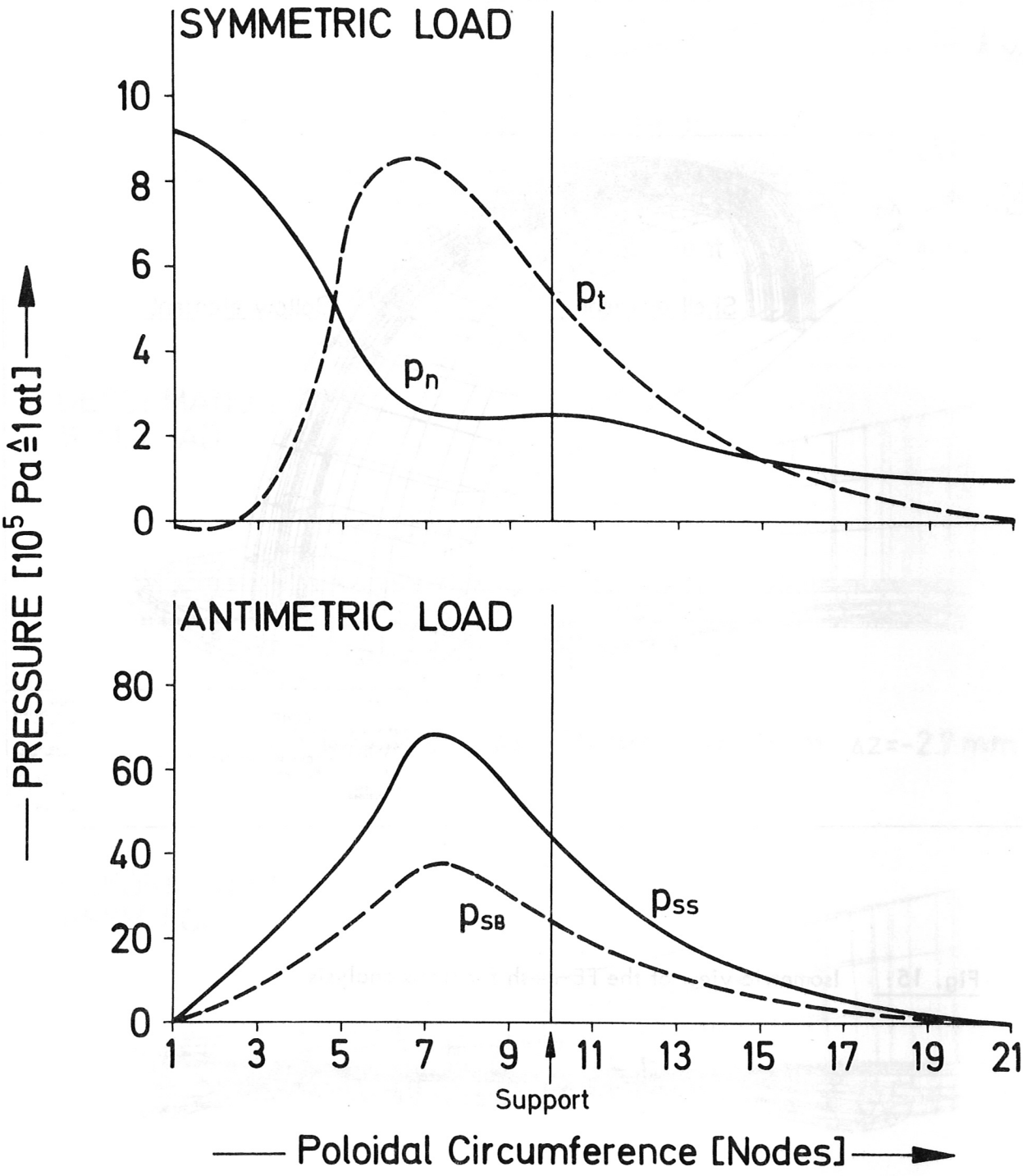

Fig. 14: Distribution of the electromagnetic loads along the poloidal circumference

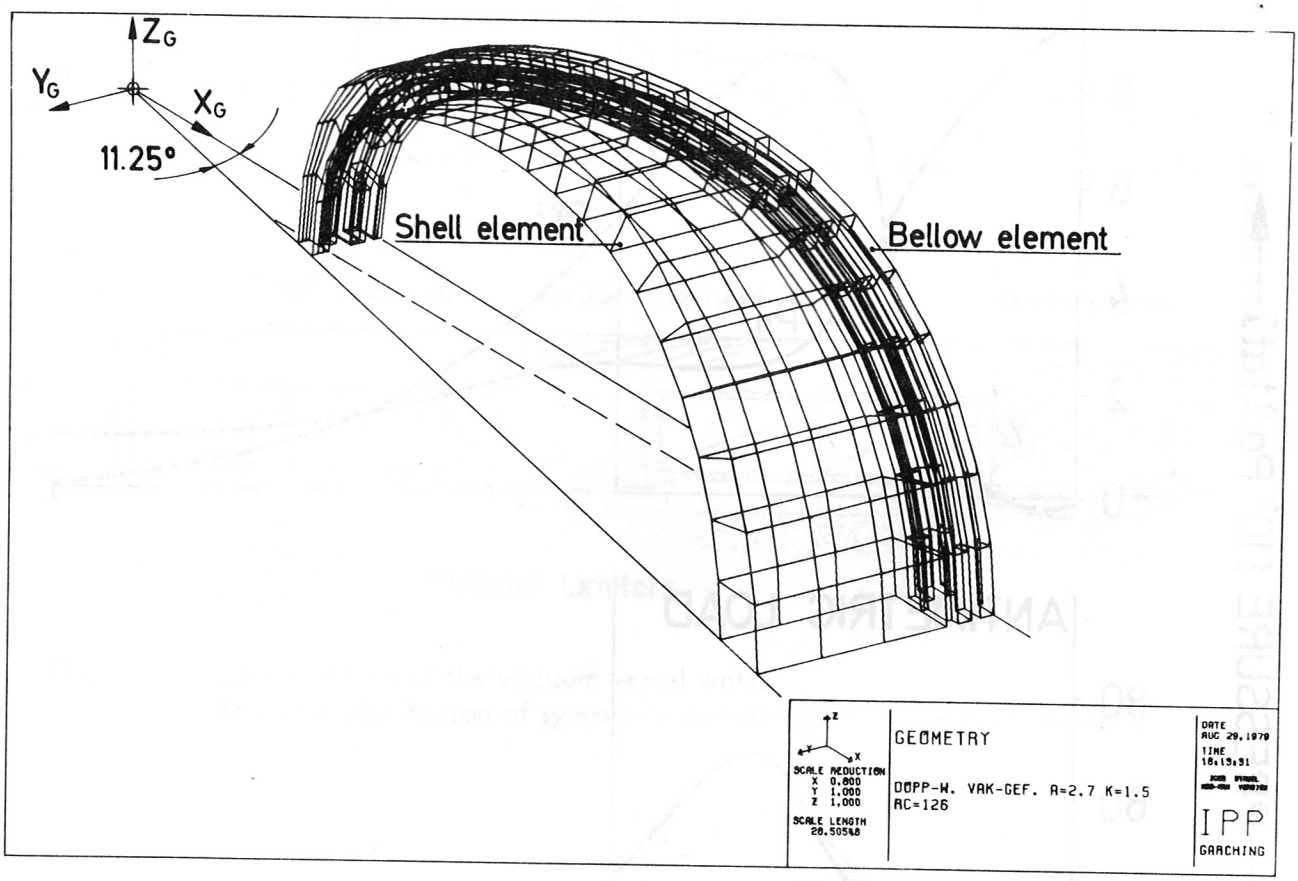

Fig. 15: Isometric view of the FE-mesh for stress analysis

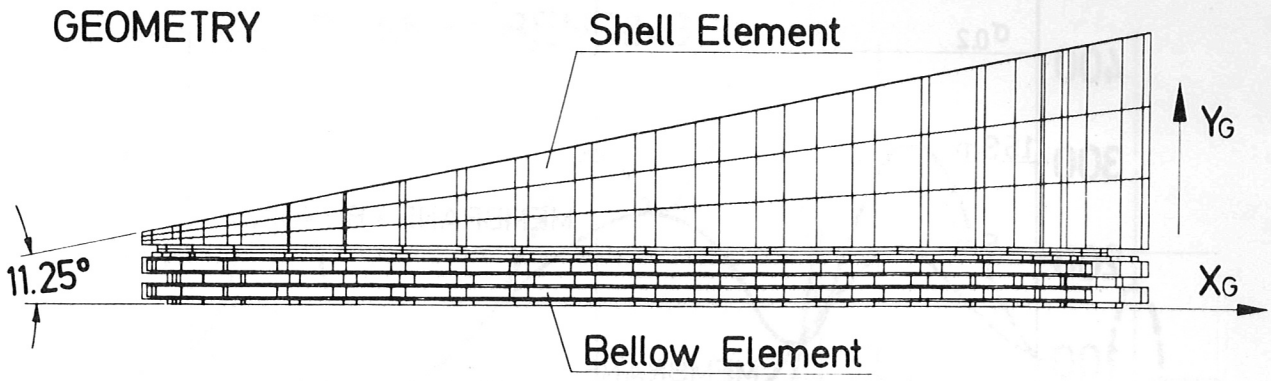

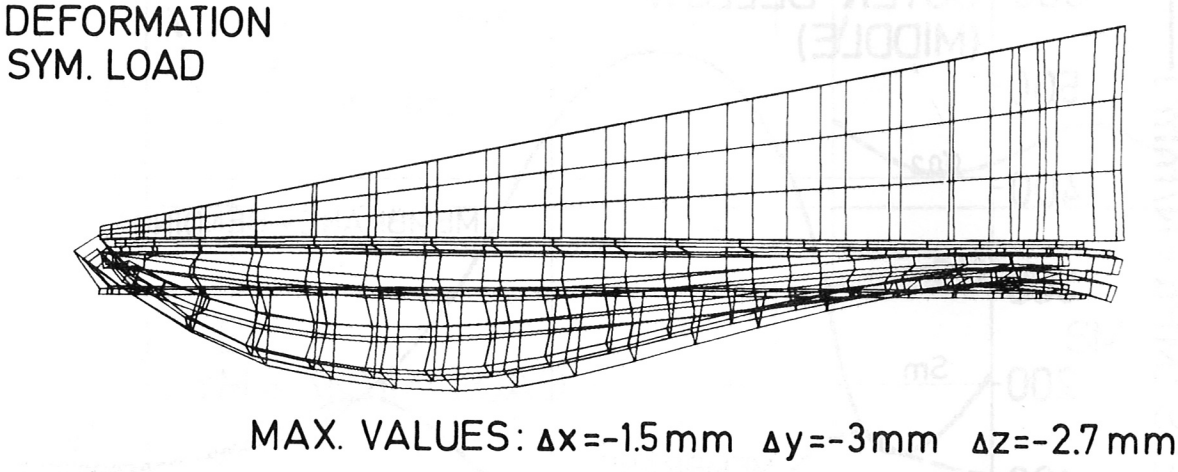

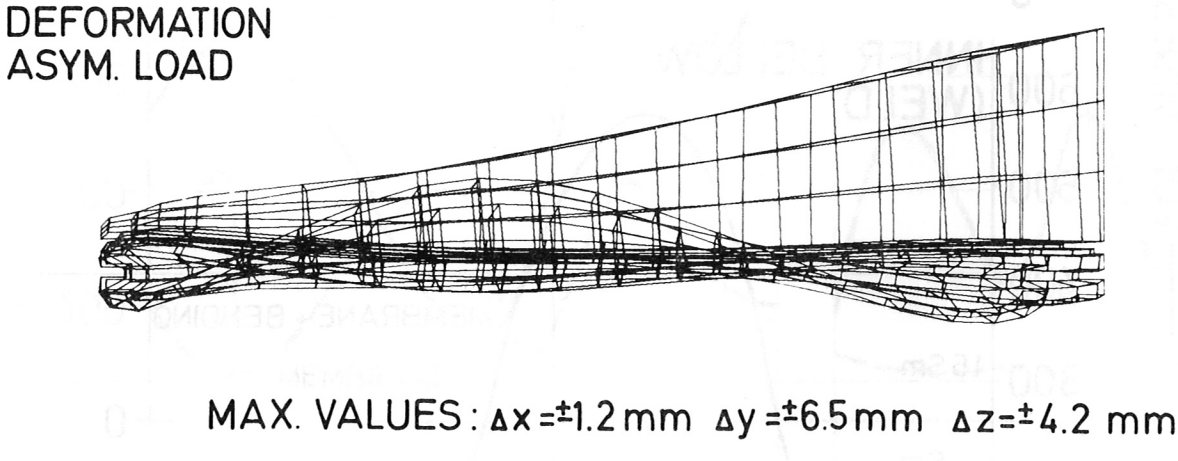

Fig. 16: Results from the stress analysis (deformations)

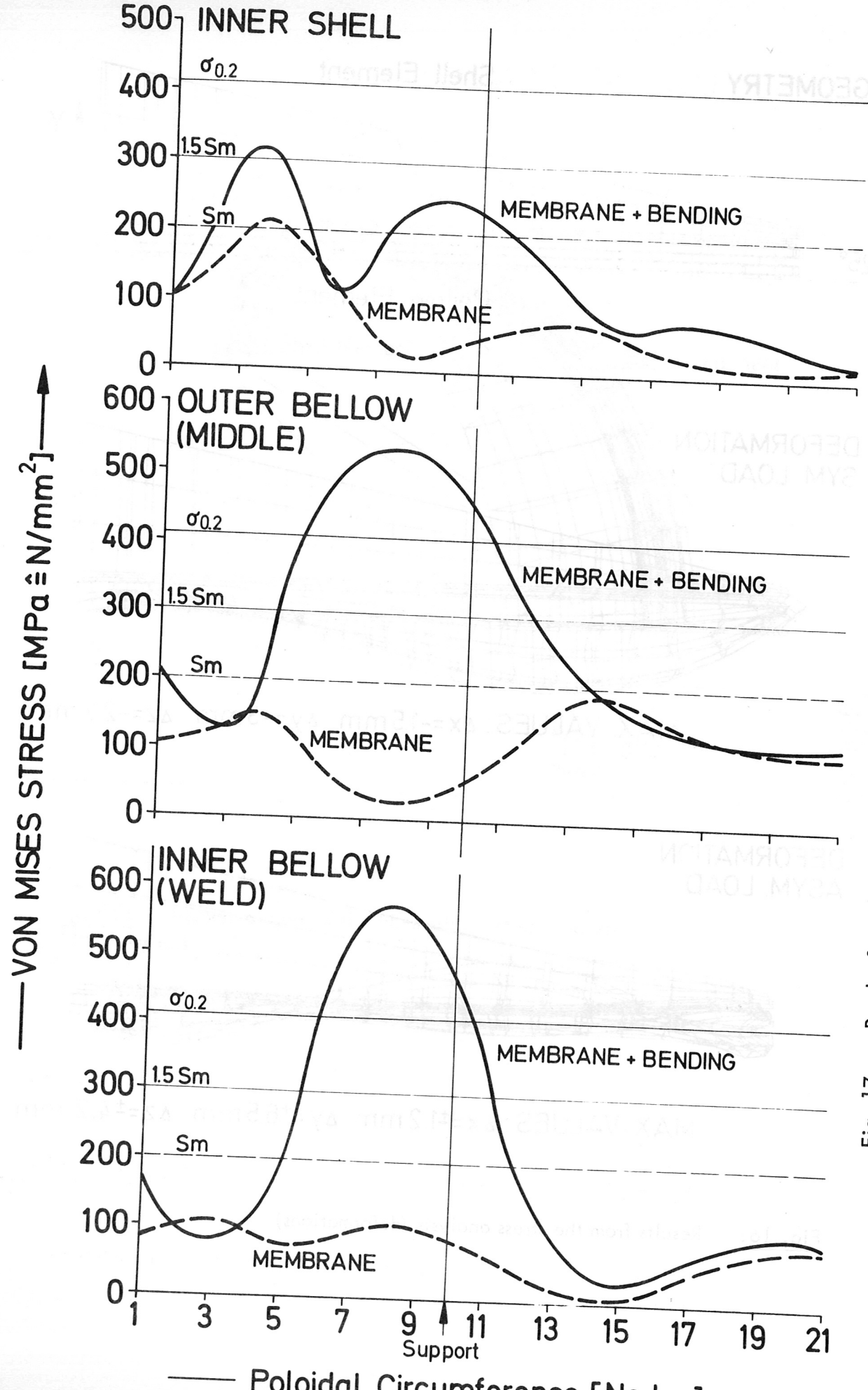

Fig. 17: Results from the stress analysis (stress distribution along the poloidal circumference

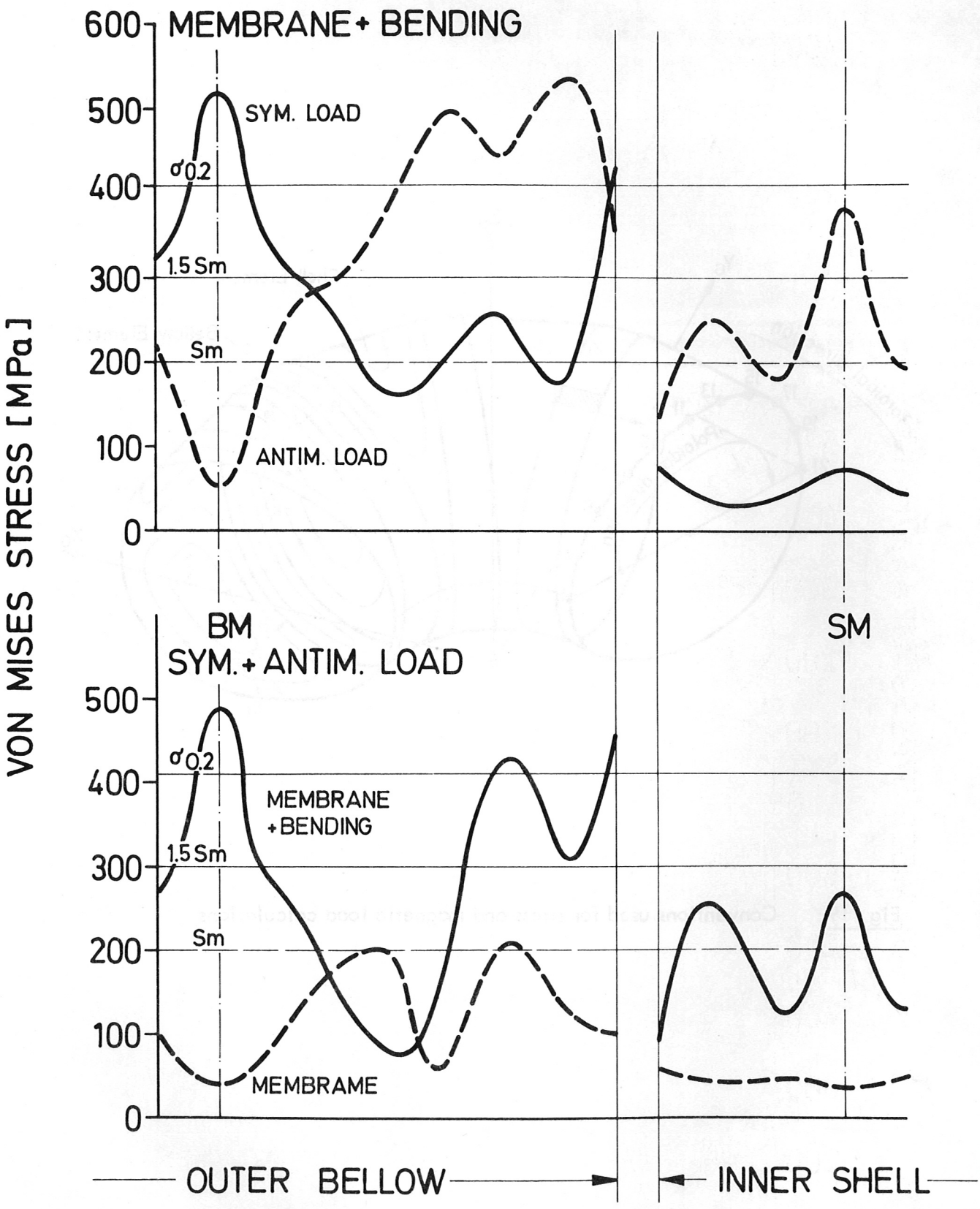

Fig. 18: Results from the stress analysis (stress distribution along the poloidal circumference

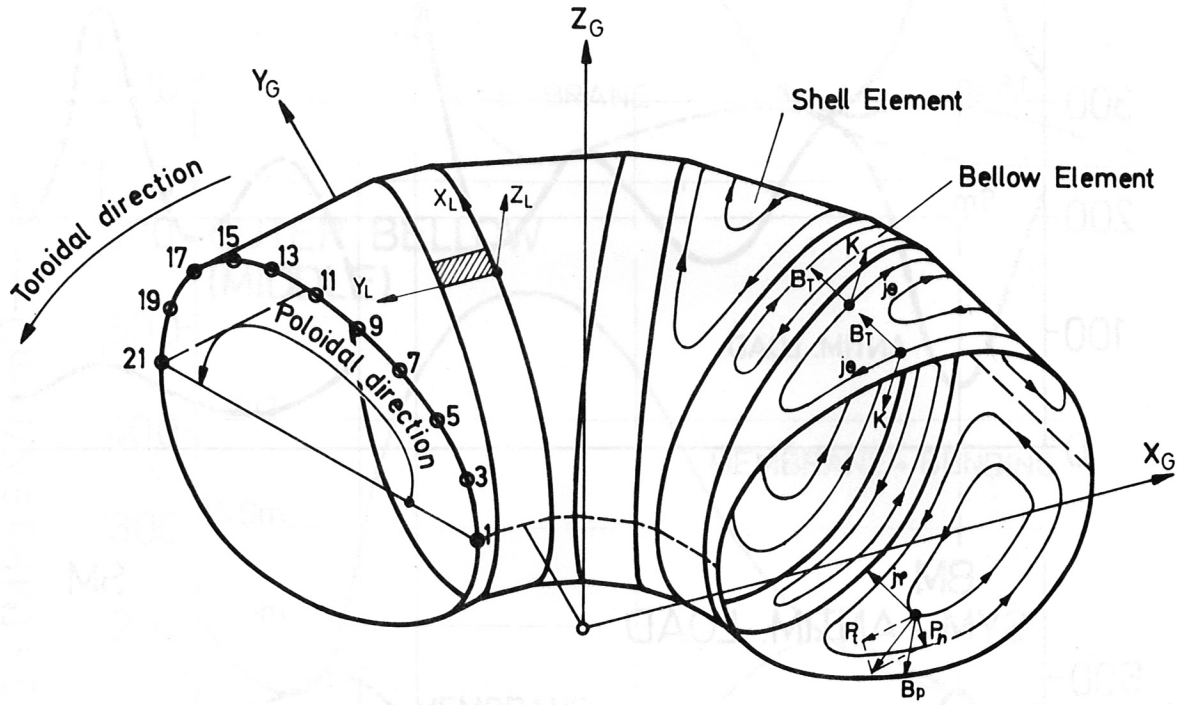

Fig. 19: Conventions used for stress and magnetic load calculations